Tracking Smoke from a Prescribed Fire and Its Impacts on Local Air Quality Using Temporally Resolved *GOES-16* ABI Aerosol Optical Depth (AOD)

AMY K. HUFF,[a] SHOBHA KONDRAGUNTA,[b] HAI ZHANG,[a] ISTVAN LASZLO,[b] MI ZHOU,[a] VANESSA CAICEDO,[c,d] RUBEN DELGADO,[c,d] AND ROBERT LEVY[e]

[a] *I. M. Systems Group, College Park, Maryland*
[b] *NOAA/NESDIS, College Park, Maryland*
[c] *Joint Center of Earth Systems Technology, University of Maryland, Baltimore County, Baltimore, Maryland*
[d] *NOAA Center for Earth System Sciences and Remote Sensing Science and Technologies, University of Maryland, Baltimore County, Baltimore, Maryland*
[e] *NASA GSFC, Greenbelt, Maryland*

(Manuscript received 9 October 2020, in final form 3 February 2021)

ABSTRACT: Aerosol optical depth (AOD) retrieved from the *GOES-16* Advanced Baseline Imager (ABI) was used to track a smoke plume from a prescribed fire in northeastern Virginia on 8 March 2020. Weather and atmospheric conditions created a favorable environment to transport the plume through the Washington, D.C., and Baltimore, Maryland, metro areas in the afternoon and concentrate smoke near the surface, degrading air quality for several hours. ABI AOD with 5-min temporal resolution and 2-km spatial resolution definitively identified the timing and geographic extent of the plume during daylight hours. Comparison to AERONET AOD indicates that ABI AOD captured the relative change in AOD due to passage of the smoke, with a mean absolute error of 0.047. Ground-based measurements of fine particulate matter ($PM_{2.5}$) confirm deteriorations in air quality coincident with the progression of the smoke. Ceilometer aerosol backscatter profiles verify plume transport timing and indicate that smoke aerosols were well mixed in a shallow boundary layer. This event illustrates the advantages of using multiple datasets to analyze the impacts of aerosols on ambient air quality. Given the quickly evolving nature of the event over several hours, ABI AOD provided information for the public and decision-makers that was not available from any other source, including polar-orbiting satellite sensors. This study suggests that $PM_{2.5}$ concentrations estimated from ABI AOD can be used to fill in the gaps in nationwide regulatory $PM_{2.5}$ monitor networks and may be a valuable addition to EPA's $PM_{2.5}$ NowCast of current air quality conditions.

KEYWORDS: Satellite observations; Surface observations; Aerosols/particulates; Air quality; Biomass burning

1. Introduction

Wildfires and prescribed fires release large amounts of smoke aerosols into the atmosphere (Wiedinmyer et al. 2006; Akagi et al. 2011; Koplitz et al. 2018), which can degrade fine particulate matter ($PM_{2.5}$) air quality and cause adverse health effects (Sapkota et al. 2005; Rappold et al. 2011; Johnston et al. 2012). In particular, prescribed fires, which are controlled burns to support land management, have been shown to be substantial sources of $PM_{2.5}$ emissions across the United States (Larkin et al. 2020). Monitors in national ambient air networks, such as State and Local Air Monitoring Stations (SLAMS), measure surface $PM_{2.5}$ concentrations to determine compliance with National Ambient Air Quality Standards (NAAQS) and other air quality regulations. The distribution of these regulatory monitors is determined by the needs of state and local air pollution management agencies to comply with State Implementation Plans (SIPs) and is nonuniform by design (U.S. Government 2017). As a result, rural areas contain few regulatory $PM_{2.5}$ monitors, which limits their utility for tracking the impacts of smoke plumes from wildfires and prescribed fires. To increase the geographic coverage of $PM_{2.5}$ air quality data, satellite aerosol optical depth (AOD) is commonly used in epidemiological and air quality modeling studies (e.g., Weber et al. 2016; Lassman et al. 2017; Stanaway et al. 2018).

AOD is a measure of the extinction (scattering and absorption) of light by aerosols in a vertical column. It is proportional to the number or mass concentration of aerosols, and thus, it is a quantitative estimate of the amount of aerosols present. Most air quality studies that incorporate satellite AOD are based on data from polar-orbiting satellite sensors such as MODIS on the *Terra* and *Aqua* satellites and VIIRS on the *SNPP* and *NOAA-20* satellites. The high accuracy and precision of MODIS AOD and VIIRS AOD products, based on multichannel AOD algorithms, are well documented (Levy et al. 2013; Liu et al. 2014; Huang et al. 2016; Laszlo and Liu 2017).

A major drawback of polar-orbiting sensors is their low temporal resolution at low and midlatitudes, where typically only 1–2 AOD observations from each sensor/satellite pair are available daily. In contrast, AOD from geostationary satellite sensors has very high temporal resolution, which permits monitoring of atmospheric aerosols on time scales of minutes to hours. In November 2016, NOAA launched the first satellite (called *GOES-16* after launch) in its new generation of geostationary

Corresponding author: Amy K. Huff, amy.huff@noaa.gov

Publisher's Note: This article was revised on 1 June 2021 to include a reprocessed version of the original Fig. 7 that improved its resolution.

DOI: 10.1175/JTECH-D-20-0162.1

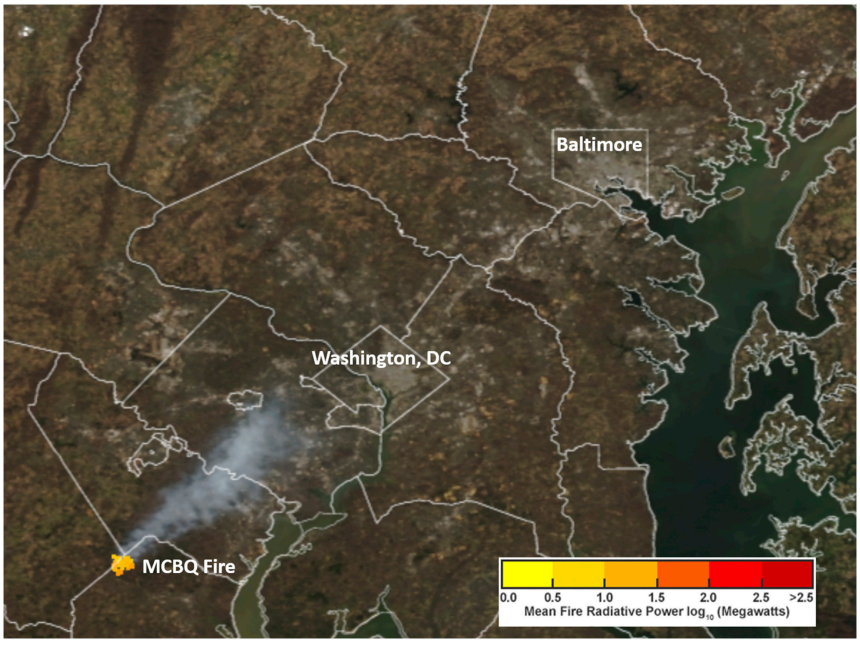

FIG. 1. *SNPP* VIIRS true color image overlaid with I-band (375-m resolution) fire radiative power, indicating the location of the prescribed fire on the lands of the Marine Corps Base Quantico (MCBQ) and its associated smoke plume at 1752–1754 UTC 8 Mar 2020.

satellites, the GOES-R series. The GOES-R satellites, including *GOES-16*, feature an Advanced Baseline Imager (ABI), which has 16 spectral bands ranging from visible to infrared (Schmit et al. 2017), thereby allowing multichannel AOD retrievals.

The ABI AOD algorithm is based on the legacy of the MODIS and VIIRS AOD dark target algorithms (Levy et al. 2007, 2010; Jackson et al. 2013; Liu et al. 2014). As a result, multichannel AOD retrieved with the ABI is expected to have accuracy analogous to that of MODIS and VIIRS AOD, but with the high temporal resolution of a geostationary satellite. The details of the ABI AOD algorithm are described by Laszlo et al. (2008) and Kondragunta et al. (2020), including the viewing conditions and data artifacts used to classify AOD retrievals as high, medium, or low quality. ABI AOD is not retrieved for pixels with invalid input data, pixels containing clouds, and for retrievals over snow/ice, bright land surface, or areas of sun glint.

GOES-16, centered at 75.2°W longitude, became operational as GOES-East in December 2017. During its routine "flex mode" scanning timeline (i.e., scan mode 6A since 2 April 2019), *GOES-16* ABI makes observations every 5 min over the CONUS sector (Schmit et al. 2017). *GOES-16* ABI AOD data have been in provisional maturity status since 14 September 2018. Provisional maturity means that product performance has been demonstrated through analysis of a small number of independent measurements, and the product is ready for operational use, but incremental product improvements may still be occurring.

A recent opportunity to showcase the high accuracy and temporal resolution of ABI AOD occurred on 8 March 2020, when a prescribed burn was conducted on the lands of the U.S. Marine Corps Base Quantico (MCBQ) in northeastern Virginia. According to press reports, the fire burned for 4 h and consumed approximately 2000 acres (Samenow 2020). The fire released a thick plume of smoke aerosols that moved along the Interstate 95 corridor from Washington, D.C., to Baltimore, Maryland, in the afternoon. Although 24-h average $PM_{2.5}$ concentrations did not exceed the daily NAAQS of 35 $\mu g\,m^{-3}$ on 8 March, the smoke degraded $PM_{2.5}$ air quality for several hours on an otherwise clean day. The location of the fire and its smoke plume at approximately 1800 UTC are shown in Fig. 1.

GOES-16 ABI AOD tracked the progress of the smoke during daylight hours. ABI AOD are compared to observations from the Goddard Space Flight Center (GSFC) AERONET station, which was in the path of the plume. Surface $PM_{2.5}$ measurements from SLAMS and the PurpleAir network, as well as aerosol backscatter profiles from ceilometers in the Unified Ceilometer Network (UCN), confirmed the trajectory of the smoke and its impact on air quality. Sounding data from Dulles International Airport (KIAD) show the meteorological conditions that set the stage for the smoke transport event.

2. Data and methodology

The analysis domain, encompassing the metropolitan region along the Interstate 95 corridor from Washington to Baltimore (referred to as the "Baltimore–Washington corridor"), is shown in Fig. 2. The location of the MCBQ fire (38.53°N, 77.55°W) is marked with a red diamond. The names, specifications, and locations of the regulatory SLAMS $PM_{2.5}$ monitors, ceilometers, and AERONET sun photometer used in this analysis are listed in Table 1. Each unique data source location is given a simple "site name," listed in Table 1 and shown in Fig. 2, to make presentation of results clear.

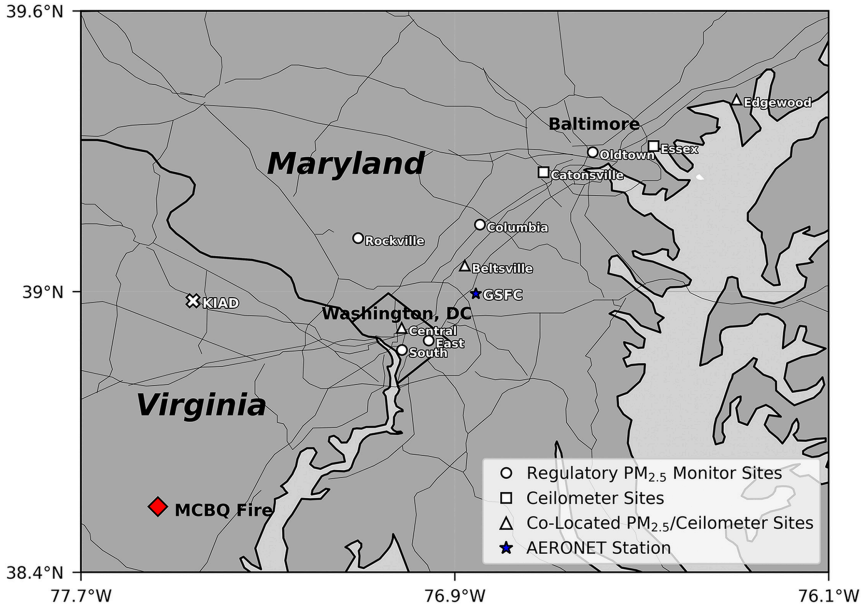

FIG. 2. Analysis domain showing the locations of the prescribed fire on the lands of the MCBQ, Dulles International Airport (KIAD), Goddard Space Flight Center (GSFC) AERONET station, ceilometers, and regulatory $PM_{2.5}$ monitors in the Baltimore–Washington metropolitan region; thin gray lines indicate state and local highways.

a. Rawinsonde observations

Archived NWS Upper-Air Observations Program rawinsonde data were downloaded from the University of Wyoming's upper-air sounding website (http://weather.uwyo.edu/upperair/sounding.html) for soundings launched from KIAD, station number 72403 (38.98°N, 77.46°W), at 1200 UTC 8 March and 0000 UTC 9 March 2020. The location of the KIAD upper-air site is indicated in Fig. 2. Observations include air temperature, dewpoint temperature, atmospheric pressure, and wind speed and direction.

b. Surface $PM_{2.5}$ concentrations

1) SLAMS REGULATORY MONITORS

Nine SLAMS Federal Equivalent Method (FEM) beta attenuation monitors (BAMs) are located in the analysis domain: five in Maryland and four in the District of Columbia (DC) (Table 1). These BAMs, henceforth referred to as regulatory monitors, continuously report 1-h average $PM_{2.5}$ concentrations. Certified hourly $PM_{2.5}$ concentration data for 8 March 2020 were provided by the Maryland Department of Environment (MDE) for the Maryland BAMs and by the DC Department of Energy and Environment (DOEE) for the DC BAMs. Due to the close geographic proximity of the Anacostia Freeway Near Road and River Terrace BAMs, data from these monitors were averaged and are reported as the DC-East site in this study.

2) PURPLEAIR SENSORS

The PurpleAir network reports measurements from low-cost commercial PurpleAir (PA-II) sensors with 2-min temporal resolution. Each PA-II unit consists of two identical Plantower PMS5003 nephelometers (termed "A" and "B"); a BME280 environmental sensor that records pressure, temperature, and humidity; and a Wi-Fi board. The nephelometers are laser optical counters that detect and count suspended particles in sizes of 0.3, 0.5, 1.0, 2.5, 5.0, and 10 μm. The proprietary PurpleAir algorithm calculates $PM_{2.5}$ mass in $\mu g\ m^{-3}$ using assumptions regarding the relative amounts of $PM_{1.0}$ to $PM_{2.5}$ based on the detected total scattered light signal. There are no corrections made to the calculated mass for temperature or humidity. The PMS5003 sensors are factory calibrated, and comparing the simultaneous readings from the identical "A" and "B" particle sensors provides a rudimentary quality control check when analyzing the data.

$PM_{2.5}$ concentration estimates from the "A" and "B" sensors (correction factor = "atm") for PurpleAir sites in the analysis domain on 8 March 2020 were downloaded from the PurpleAir website (https://www2.purpleair.com/) using the Chrome downloader tool. After removing sites with >25% missing data, sites with >10% difference between "A" and "B" sensor values, and sites for which data were not available during the entire smoke transport event period (1800–2300 UTC), 56 sites remained for analysis. For each of these sites, 2-min observations were aggregated to 1-h intervals, and data from the A and B sensors were averaged.

PurpleAir sensors have a known high bias for measurement of smoke aerosols (e.g., Gupta et al. 2018; Holder et al. 2020). The PurpleAir 1-h average $PM_{2.5}$ concentrations ($[PM]_{Sensor}$) were corrected for this bias using the sensor-specific optimized simple linear correction equation for wildfire smoke developed by Holder et al. (2020):

$$[PM_{2.5}]_{Corrected} = 0.79 \times [PM_{2.5}]_{Sensor} - 7.96. \quad (1)$$

TABLE 1. Names, specifications, and locations of regulatory $PM_{2.5}$ monitors, ceilometers, and AERONET sun photometer used in the analysis. $PM_{2.5}$ monitors maintained by Maryland Department of Environment (MDE) are indicated by one asterisk (*) and those maintained by DC Department of Energy and Environment (DOEE) are indicated by two asterisks (**).

Site name	Latitude (°N)	Longitude (°W)	Regulatory $PM_{2.5}$ monitor	Ceilometer	AERONET sun photometer
Beltsville	39.0553	76.8783	HU-Beltsville* (MetOne BAM 1020)	Lufft CHM15k (1064 nm)	—
Catonsville	39.2550	76.7095	—		—
Columbia	39.1432	76.8462	Howard County Near Road* (MetOne BAM 1020)	—	—
DC-Central	38.9218	77.0132	McMillian Reservoir** (MetOne BAM 1022)	Vaisala CL51 (910 nm)	—
DC-East	38.8952	76.9558	Anacostia Freeway Near Road** (MetOne BAM 1022)	—	—
			River Terrace** (MetOne BAM 1022)		—
DC-South	38.8752	77.0128	King Greenleaf Recreation Center** (MetOne BAM 1022)	—	—
Edgewood	39.4102	76.2967	Edgewood* (MetOne BAM 1020)	Vaisala CL51 (910 nm)	—
Essex	39.3108	76.4744	—	Lufft CHM8k (905 nm)	—
GSFC	38.9925	76.8398	—	—	Goddard Space Flight Center
Oldtown	39.2981	76.6047	Oldtown* (MetOne BAM 1020)	—	—
Rockville	39.1144	77.1069	Rockville* (MetOne BAM 1020)	—	—

Holder et al. (2020) report a mean absolute error (MAE) of 7.68 $\mu g\,m^{-3}$ for PurpleAir sensor $PM_{2.5}$ concentrations corrected using Eq. (1) ($[PM_{2.5}]_{Corrected}$).

c. *Ceilometer aerosol backscatter and mixing layer height*

Five ceilometers in the UCN (https://alg.umbc.edu/ucn/), a ground-based ceilometer network collaboration between the University of Maryland, Baltimore County (UMBC), EPA, and NASA, are located in the analysis domain (Table 1).

Ceilometer data in this study demonstrate the vertical extent and movement of the MCBQ plume through the Baltimore–Washington corridor. Quantitative comparison of aerosol/particle backscatter magnitude is hindered due to variations in the design, laser wavelength, and aerosol backscatter derivation methodologies of the different ceilometer models in the UCN (Table 1) (Heese et al. 2010; Cazorla et al. 2017). PBL heights (Table 2) were retrieved using the Haar wavelet covariance transform methodology described by Caicedo et al. (2020).

d. *AERONET AOD*

AERONET is a global ground-based remote sensing aerosol network of sun photometers that measure spectral sun irradiance and sky radiances (Holben et al. 1998), which are used to retrieve aerosol properties, including AOD. AERONET AOD is ground truth for validation of satellite AOD retrievals (Holben et al. 1998).

Two AERONET stations are located in the analysis domain: GSFC (38.9925°N, 76.8398°W) and Maryland Science Center (39.212°N, 76.6121°W). The GSFC station observed the passage of the smoke plume, but it reached the Maryland Science Center site too late in the day for AOD to be retrieved.

AERONET, version 3, level 1.5 data from the GFSC station on 8 March 2020 were downloaded using the AERONET Data Download Tool (https://aeronet.gsfc.nasa.gov/cgi-bin/webtool_aod_v3). Level 1.5 data were used because fully quality assured level 2.0 data were not available at the time of analysis. Downloaded data used in this analysis included AERONET AOD measured at 340, 380, 440, 500, 675, 870, 1020, and 1640 nm and Ångström exponent (AE) at 440–675 nm. To make direct comparison to ABI AOD, which is measured at 550 nm, AERONET AOD at 550 nm was interpolated from AERONET AOD observations at 340, 380, 440, 500, 675, 870, 1020, and 1640 nm.

e. GOES-16 *ABI AOD*

GOES-16 ABI CONUS sector AOD data for 8 March 2020 were postprocessed to remove a diurnal bias in the current provisional maturity AOD retrievals (Zhang et al. 2020). Data quality flags were used to isolate high and medium quality AOD retrievals (“top 2 qualities”) for analysis. AOD data have 2-km spatial resolution at nadir and 5-min temporal resolution. The valid AOD range is [−0.05, 5]. Negative AOD values represent the uncertainty in the AOD measurement and can be considered as very small positive AOD. To facilitate comparison to 1-h average $PM_{2.5}$ concentration data, 5-min ABI AOD observations were averaged to 1-h composites.

ABI AOD were compared to AERONET AOD using the spatiotemporal collocation methodology of the Multisensor Aerosol Products Sampling System (MAPSS) (Petrenko et al. 2012), which is the standard protocol for averaging satellite data in time and space for comparison to ground-based observations. Following the MAPSS approach, all ABI AOD pixels within a circle of 27.5-km radius, centered on the AERONET station, were spatially averaged for each 5-min AOD time step, with a minimum of 120 pixels (~20%) required for a valid matchup. These spatially matched ABI AOD averages were temporally matched with AERONET AOD in a 1-h time window (±30 min), centered on the ABI observation time.

The MAPSS spatiotemporal matching approach was used to compare ABI AOD to $PM_{2.5}$ concentrations at the four regulatory

TABLE 2. Information on approximate smoke plume arrival and departure times and maximum height of the planetary boundary layer (PBL) on 8 Mar 2020, derived from ceilometer measurements.

Site name	Smoke arrival time (UTC)	Smoke departure time (UTC)	Maximum PBL height (km)
DC-Central	1840	2100	1.230
Beltsville	2000	2200	1.124
Catonsville	2110	2300	1.213
Essex	2200	2330	1.203
Edgewood	2230	2350	0.990

monitor sites (e.g., Beltsville, Columbia, DC-Central, Rockville) that were impacted by the smoke plume during daylight hours, when ABI AOD retrievals were made. Spatially and temporally matched ABI AOD averages at approximately 5-min resolution were averaged to 1 h to match the resolution of the 1-h average $PM_{2.5}$ concentration data. The DC-Central site was chosen as a representative location in DC to avoid redundancy, given that ABI AOD spatial averaging at the three $PM_{2.5}$ monitor sites in DC would result in nearly identical AOD matchups.

3. Results

a. *Meteorological and atmospheric conditions on 8 March 2020*

The MCBQ prescribed fire was a ''back burn'' conducted at 1500–1900 UTC 8 March 2020 to ''control wildfires set by troop training,'' according to posts on the Facebook account of the Quantico Fire and Emergency Services, since deleted (Samenow 2020). Skew *T*–log*p* plots of rawinsonde data from the KIAD upper air station at 1200 UTC 8 March (Fig. 3a) and 0000 UTC 9 March (Fig. 3b) show the meteorological conditions at Dulles International Airport, located approximately 40.5 km from the MCBQ fire and 40.0 km from downtown Washington, DC.

The temperature on 8 March was warmer than average for early March. The maximum temperature at KIAD was 17.2°C, nearly 6°C above the historical daily normal maximum temperature of 11.4°C for 8 March (NOAA NCDC Climate Data Online; https://www.ncdc.noaa.gov/). The 0000 UTC sounding shows that surface air temperature was 15.4°C, indicating the warmth lingered through the late afternoon and early evening. The air was also extremely dry. The 1200 UTC sounding indicates a very dry layer just above the surface, with dewpoints dropping from −5.5°C at the surface to −32.6°C at 925 hPa. A strong temperature inversion from the surface to 959 hPa (0.615 km) is evident in the 1200 UTC sounding, as well as a secondary inversion aloft from 867 to 801 hPa (1.430–2.064 km). The near-surface inversion broke once the surface air temperature reached approximately 10°C, allowing the very dry air aloft to mix down and push the surface dewpoint to −14.4°C in the afternoon (1800 UTC), which resulted in a very low surface RH of approximately 12%. The warm and dry conditions were favorable for the biomass fuel to burn and produce smoke. Research has shown that smoke from prescribed burns in the January to April time frame can contain sufficient moisture to promote formation of polluted dense fog at night (Achtemeier 2009). Since the MCBQ fire and subsequent smoke transport occurred during the daytime, smoke moisture-induced fog was unlikely.

The predominant winds blew the smoke from the MCBQ fire through the Baltimore–Washington corridor. The 1200 UTC sounding shows calm winds at the surface in the morning; westerly winds (260°–280°) at 5–10 kt (~2.6–5.1 m s^{-1}) mixed down after the near-surface inversion broke. By 0000 UTC, surface winds were 8–10 kt (~4.1–5.1 m s^{-1}) and had shifted to the south (180°–190°). Southwesterly winds in the afternoon

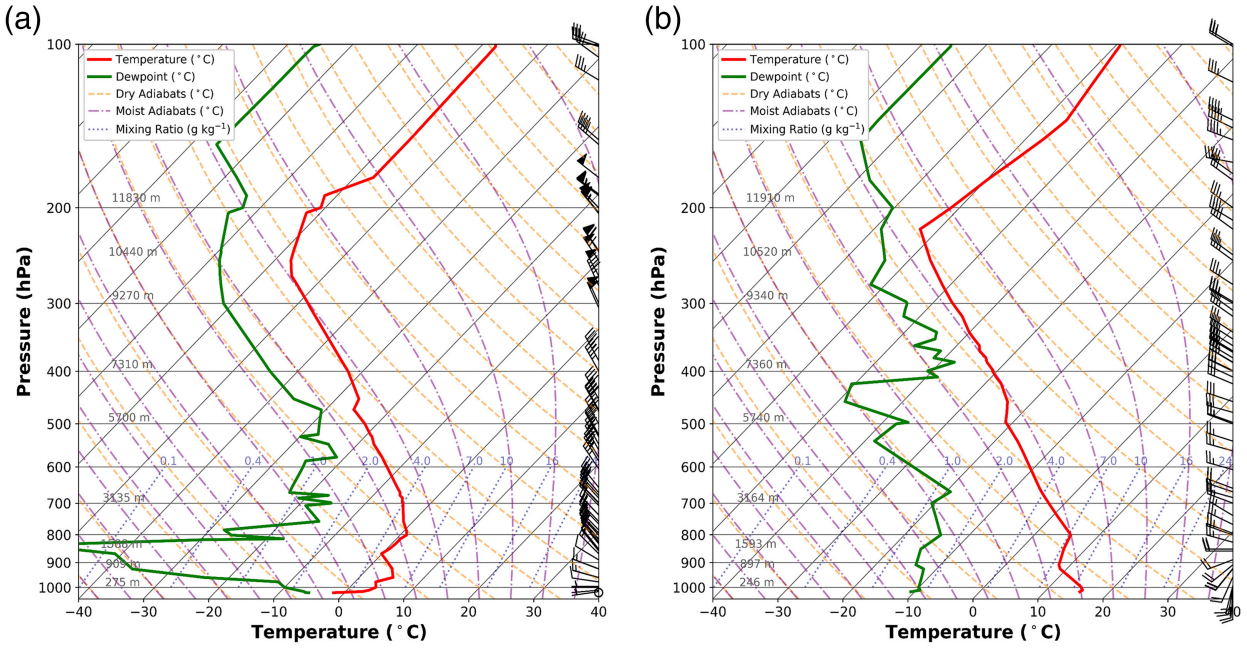

FIG. 3. Skew *T*–log*p* plots of rawinsonde data from the KIAD upper-air station at (a) 1200 UTC 8 Mar and (b) 0000 UTC 9 Mar 2020.

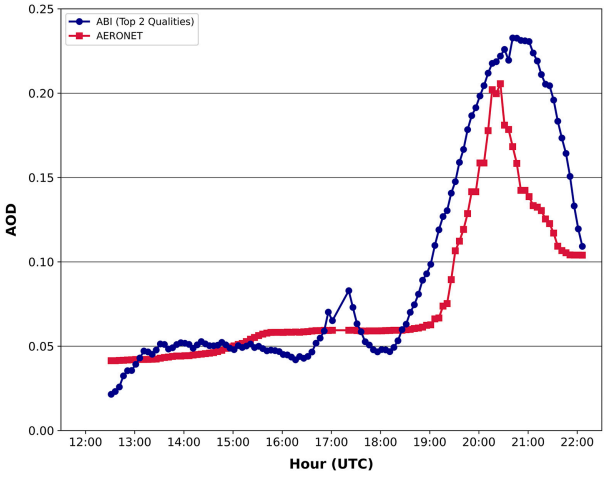

FIG. 4. Time series of AERONET AOD (550 nm) and *GOES-16* ABI AOD (550 nm) from 8 Mar 2020 at the GSFC station.

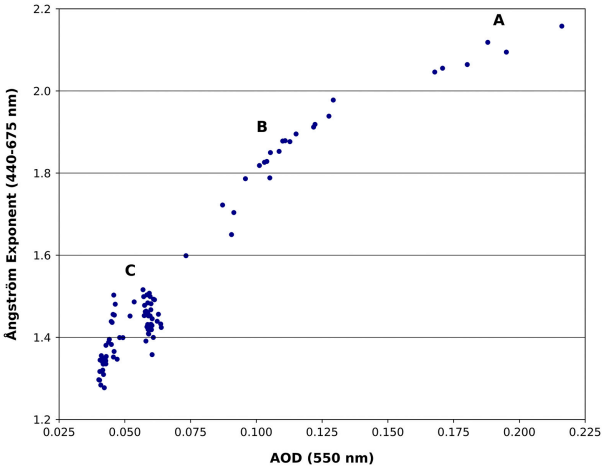

FIG. 5. Scatterplot of AERONET AOD (550 nm) and Ångström exponent (440–675 nm) from 8 Mar 2020 at the GSFC station; data cluster "A" corresponds to biomass burning aerosols, "B" to mixed aerosols, and "C" to clean continental aerosols (with high uncertainty given very low AOD values) based on aerosol type categories defined by Kumar et al. (2015) and Filonchyk et al. (2020).

transported smoke from the MCBQ fire northeastward to Washington, through the Maryland suburbs between DC and Baltimore along Interstate 95, and finally to downtown Baltimore by sunset.

Limited vertical mixing on 8 March trapped the smoke near the surface, intensifying its impacts on air quality. The 0000 UTC sounding confirms that the morning near-surface inversion broke, but the secondary inversion aloft capped the PBL to a maximum height of approximately 1.4 km. Estimated maximum PBL heights derived from ceilometer measurements (Table 2) confirm that vertical mixing in the afternoon was limited to a maximum of 1.1–1.2 km along the path of the transported smoke plume.

b. *Comparison of AERONET and ABI AOD*

The time series of AERONET AOD and ABI AOD at the GSFC station on 8 March 2020 is shown in Fig. 4. AERONET and ABI AOD are computed at 550 nm, so data are only available during daylight hours. In addition, ABI AOD retrieved under conditions of solar zenith angle $> 80°$ are considered unreliable and are designated as low quality; top two qualities ABI AOD observations spanned from 1231 to 2211 UTC in the analysis domain on 8 March.

The very low AERONET AOD values of 0.04–0.06 throughout the morning and early afternoon illustrate that air quality was very clean prior to the arrival of the MCBQ plume. No transport of particle pollution from upwind occurred on 8 March. In addition, it was a Sunday, with lower local emissions compared to Monday–Saturday.

AERONET AOD indicates that the MCBQ plume reached the GSFC station at approximately 1900 UTC, when AOD increases sharply from an average of 0.05 (1231–1901 UTC) to a maximum of 0.21 at 2026 UTC, before falling to near 0.10 at 2206 UTC when retrievals stopped due to the impending sunset.

Postprocessed ABI AOD retains a small diurnal bias, which peaked at 1721 UTC with a maximum AOD of 0.083. This temporary increase in ABI AOD occurred before the arrival of the MCBQ plume, so it does not interfere with the change in AOD associated with the smoke. Consequently, ABI AOD observes the full cycle of response due to the passing plume at GSFC, with ABI AOD sharply increasing beginning at 1826 UTC, reaching a maximum of 0.23 at 2041 UTC, and then decreasing steadily to 0.11 by the last observation at 2206 UTC. The shape of the ABI AOD peak mirrors that of AERONET AOD, but ABI AOD is consistently higher than AERONET by an average of 0.047 during the smoke detection period (1826–2206 UTC). In addition, ABI AOD reaches a maximum due to the smoke about 15 min later than AERONET.

The scatterplot of AERONET AOD at 550 nm and AE at 440–675 nm observed at the GSFC station (Fig. 5) confirms that the pulse of high AOD aerosols associated with the MCBQ plume was smoke. AE is a qualitative indicator of aerosol size distribution (Eck et al. 1999). AE is inversely related to particle size; smaller aerosols, such as smoke, have higher values of AE compared to larger aerosols, such as dust. AE in conjunction with AOD can be used to group aerosols into broad categories of aerosol types (e.g., Ciren and Kondragunta 2014; Kumar et al. 2015; Filonchyk et al. 2020). In Fig. 5, aerosols with AOD ≥ 0.075 have AE values spanning approximately 1.6–2.1, spreading out in an arc toward the upper right corner of the plot. These data represent the concurrent increase in AOD and decrease in particle size for aerosols corresponding to the passage of the smoke plume (Eck et al. 1999). Using the aerosol type categories developed by Kumar et al. (2015) and Filonchyk et al. (2020), data with AOD approximately 0.175–0.225 and AE > 2.0 (cluster "A" in Fig. 5) roughly correspond to biomass burning aerosols, while data with AOD approximately 0.075–0.125 and AE 1.6–2.0 (cluster "B" in Fig. 5) are mixed aerosols. The data cluster with AOD < 0.075 and AE approximately 1.3–1.5 ("C" in Fig. 5) suggest clean continental aerosols prior to the arrival of the MCBQ plume, but AE for such low AOD values has high uncertainty (Eck et al. 1999).

Comparison to AERONET AOD demonstrates that ABI AOD accurately captured the relative change in AOD due to the smoke, with a MAE of 0.047 (averaged over 220 min) at GSFC. This value compares well to the ABI AOD retrieval performance requirements. For an AOD range of 0.04–0.8, the accuracy requirement for retrievals over land is 0.04 (Kondragunta et al. 2020). Official verification metrics are compiled over a statistically large sample size covering all seasons, so a MAE for one site averaged over only a few hours that is comparable to the official requirement lends confidence in the use of ABI AOD to track the movement of the MCBQ plume through the Baltimore–Washington corridor on 8 March and assess its impacts on surface $PM_{2.5}$ air quality.

c. *Transport of smoke and impacts on surface $PM_{2.5}$*

Ceilometer aerosol backscatter profiles for the DC-Central (Fig. 6a), Beltsville (Fig. 6b), Catonsville (Fig. 6c), Essex (Fig. 6d), and Edgewood (Fig. 6e) sites show the progression of the MCBQ plume through the analysis region and the approximate times of smoke arrival and departure at each station (summarized in Table 2) along with the estimated PBL height (black line).

The fact that 8 March was a very clean day prior to the arrival of the MCBQ plume makes the change in aerosol backscatter intensity associated with the smoke aerosols in the PBL very easy to discern. At each site, the arrival of the plume corresponds to an increase in aerosol backscatter intensity in the PBL, with a subsequent decrease when the plume departs.

The aerosol backscatter profiles clearly show the smoke was trapped near the surface and well mixed in a relatively shallow PBL on 8 March at all sites except Edgewood. The profile in Fig. 6e indicates that the plume did move through Edgewood at approximately 2230–2350 UTC, but the smoke did not reach the surface. Values of $\log_{10}$ of aerosol backscatter < 2.5 below ~200-m altitude in Fig. 6e denote that the smoke remained aloft, likely because by the time the plume reached Edgewood, the nocturnal surface layer had formed, sealing off the surface from the smoke. $PM_{2.5}$ measurements from the Edgewood monitor (Fig. 7) support the ceilometer data for 1800–2200 UTC. In fact, 1-h average $PM_{2.5}$ at Edgewood remained $\leq 5\,\mu g\,m^{-3}$ for the entire period of 1200–2300 UTC, indicating no impact from the transported smoke plume.

An aerosol plume is also evident in Fig. 6 at each ceilometer site at about 1.5–3.0-km altitude from ~1200 to 2300 UTC, representing transport of aerosols of unknown origin from upwind in the residual layer. Since this unknown plume is located above the PBL, it cannot be related to the MCBQ fire. The unknown plume was not detected by ABI AOD or AERONET AOD at GSFC.

Since the smoke was well mixed in the PBL, it impacted surface air quality as it moved through the Baltimore–Washington corridor, and the timing of plume transport denoted by ABI AOD matches that from the ceilometer profiles. Maps of 1-h composite ABI AOD overlaid with corresponding 1-h average $PM_{2.5}$ from regulatory monitors and PurpleAir sensors are shown in Fig. 7 for 1800–2100 UTC. Times are given as beginning hours, meaning that for example, 1800 UTC corresponds to the average of observations for 1800–1859 UTC. Also included in Fig. 7 is a map of 1-h average $PM_{2.5}$ for 2200 UTC; ABI AOD retrievals ended at 2216 UTC due to the impending sunset, so there is no corresponding 1-h composite ABI AOD for 2200 UTC (Fig. 7e).

ABI AOD shows that at 1800 UTC (Fig. 7a), the leading edge of the MCBQ plume had reached southern DC, with AOD values ~0.25–0.30 (green shading). $PM_{2.5}$ measured by regulatory monitors in DC was $<10\,\mu g\,m^{-3}$, confirming minimal impact from the smoke. The thickest part of the plume (AOD 0.50–0.80) was located in northern Virginia, near the border with DC, where PurpleAir sensors measured high $PM_{2.5}$ ($>75\,\mu g\,m^{-3}$). Elsewhere, $PM_{2.5}$ concentrations were very low ($<5\,\mu g\,m^{-3}$), consistent with ABI observations of very low AOD in areas outside of the smoke plume.

At 1900 UTC (Fig. 7b), AOD indicates the leading portion of the plume had expanded eastward, in addition to the entire plume continuing to move gradually northward. This shift is due to an increase in southwesterly surface winds, confirmed by data from MDE's radar wind profiler at the Beltsville site (https://madis-data.bldr.ncep.noaa.gov/cap/profiler.jsp?options=full). During this hour, almost the entirety of DC was encompassed by thick smoke, with AOD of 0.30–0.60. Correspondingly, $PM_{2.5}$ at the regulatory monitors in DC surged to 14–30 $\mu g\,m^{-3}$. The number of PurpleAir sensors in northern Virginia with high $PM_{2.5}$ ($>75\,\mu g\,m^{-3}$) increased coincident with the expanding area of thicker smoke delineated by the AOD. North of the plume, along Interstate 95 and in Baltimore, $PM_{2.5}$ concentrations remained very low ($<5\,\mu g\,m^{-3}$).

At 2000 UTC (Fig. 7c), the eastward expansion of the plume was still pronounced. The thickest smoke was located over the Maryland suburbs north of DC, with maximum AOD values persisting in the 0.30–0.60 range. The Beltsville monitor, in the midst of the thick smoke, surged to 44 $\mu g\,m^{-3}$. On the leading edge of the plume, the Columbia monitor rose to 17 $\mu g\,m^{-3}$. Although the trailing edge of thick smoke remained over northern DC, the plume had pulled away from central, eastern, and southern DC, where the regulatory $PM_{2.5}$ monitors dropped below 15 $\mu g\,m^{-3}$ at all three DC sites. In the Baltimore metro area, ahead of the smoke plume, $PM_{2.5}$ remained very low ($<5\,\mu g\,m^{-3}$).

At 2100 UTC (Fig. 7d), AOD shows that the smoke plume continued drifting northeast. The geographic extent of the highest AOD values decreased, with no AOD > 0.55 and only a relatively small area of AOD = 0.45–0.55, indicating that the thickest smoke had dispersed relative to the previous 3 h. The Columbia monitor, located in the part of the plume with the highest AOD and presumably the thickest smoke, reached 66 $\mu g\,m^{-3}$, which was the highest reading from a regulatory monitor during the event. As the tail of the plume moved over the Maryland suburbs north of DC, the Rockville monitor rose to 35 $\mu g\,m^{-3}$. In contrast, the Beltsville monitor dropped to 20 $\mu g\,m^{-3}$ as the main part of the plume pulled away to the north. AOD indicates that the leading edge of the plume moved into the southern part of the Baltimore metro area (green shading). The PurpleAir sensors in the central and southern portions of downtown Baltimore increased in response to the advancing smoke, although the Oldtown

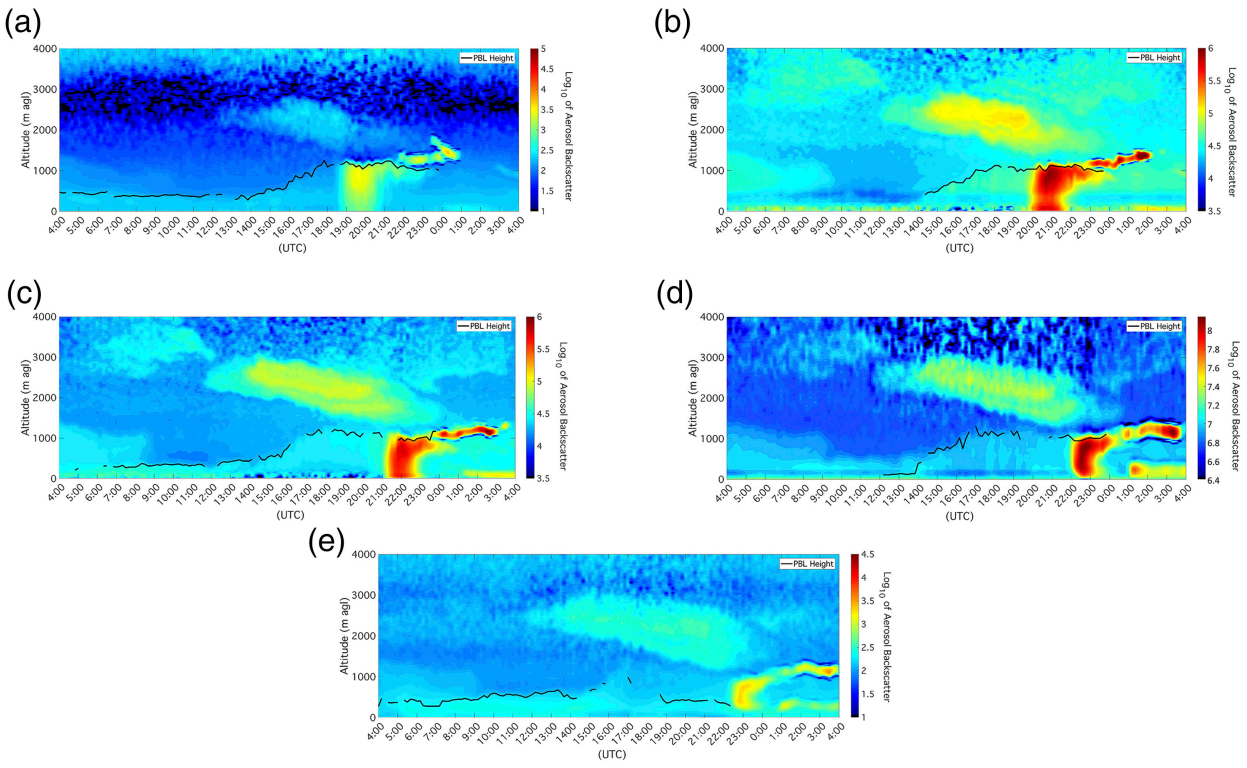

FIG. 6. Ceilometer aerosol backscatter profiles from the (a) DC-Central, (b) Beltsville, (c) Catonsville, (d) Essex, and (e) Edgewood sites on 8 Mar 2020. Differences in aerosol backscatter intensities are due to varying laser wavelength and retrieval techniques among the different instruments used at the sites (Table 1).

monitor remained very low ($3\,\mu g\,m^{-3}$). In DC, the regulatory monitors dropped to near presmoke values ($<7\,\mu g\,m^{-3}$), corresponding to the departure of the smoke plume as indicated by AOD < 0.10 (cyan shading).

With the loss of AOD retrievals at 2211 UTC due to impending sunset, tracking the continued movement of the smoke plume with satellite observations was not possible. $PM_{2.5}$ measurements (Fig. 7e) suggest that the smoke plume progressed into the Baltimore metro area in the 2200 UTC hour. The Oldtown monitor spiked to $53\,\mu g\,m^{-3}$, while the surrounding PurpleAir sensors recorded $PM_{2.5} > 50\,\mu g\,m^{-3}$. The Rockville monitor dropped slightly to $23\,\mu g\,m^{-3}$ but was still being impacted by the tail of the smoke plume. $PM_{2.5}$ at the Beltsville and DC regulatory monitors decreased to $<5\,\mu g\,m^{-3}$, indicating that the smoke had completely cleared those sites. PurpleAir measurements suggest that the rest of DC and northern Virginia had also cleaned out in the wake of the plume.

As demonstrated in Fig. 7, ABI AOD provides a regional view of the MCBQ plume. To evaluate the relationship between AOD and $PM_{2.5}$ concentration directly, Fig. 8 shows the daily time series of 1-h average ABI AOD and corresponding 1-h average $PM_{2.5}$ concentrations from the monitors at DC-Central (Fig. 8a), Beltsville (Fig. 8b), Columbia (Fig. 8c), and Rockville (Fig. 8d). Prior to 1700 UTC, AOD and $PM_{2.5}$ were very low at all of the sites. In fact, $PM_{2.5}$ was at or slightly below $0\,\mu g\,m^{-3}$ at the Beltsville, Columbia, and Rockville monitors for 4–6 consecutive hours before the arrival of the smoke at 1900–2000 UTC. Negative $PM_{2.5}$ values as low as $-10\,\mu g\,m^{-3}$ are valid for regulatory monitors and occur when the atmosphere is very clean, and there is noise in the $PM_{2.5}$ BAM measurement.

Given the backdrop of very clean conditions through the early afternoon, the surge in ABI AOD and $PM_{2.5}$ concentrations at all four sites evident in Fig. 8 is entirely attributable to smoke in the transported MCBQ plume. At each site, AOD and $PM_{2.5}$ rose in response to the arrival of the plume, attained maximum values corresponding to the presence of the thickest smoke, and then decreased as the plume moved away. Although the cycle of AOD response to the smoke (increase, maximum, and decrease) mirrored that of $PM_{2.5}$ at each site, the timing of the cycles varied slightly. At DC-Central, the peak in AOD (0.23 at 2000 UTC) lagged that of $PM_{2.5}$ ($24.5\,\mu g\,m^{-3}$ at 1900 UTC) by 1 h. At Beltsville and Columbia, the AOD and $PM_{2.5}$ peaks coincided, with maxima of 0.23 and $44\,\mu g\,m^{-3}$ at Beltsville (2000 UTC) and of 0.22 and $66\,\mu g\,m^{-3}$ at Columbia (2100 UTC). At Rockville, the peak in AOD (0.19 at 2000 UTC) preceded that of $PM_{2.5}$ ($35\,\mu g\,m^{-3}$ at 2100 UTC) by 1 h.

4. Discussion

Sunday, 8 March 2020 was an unsuitable day to conduct a prescribed burn at a location southwest of the heavily populated Baltimore–Washington corridor. Warm and very dry weather conditions promoted smoke production from

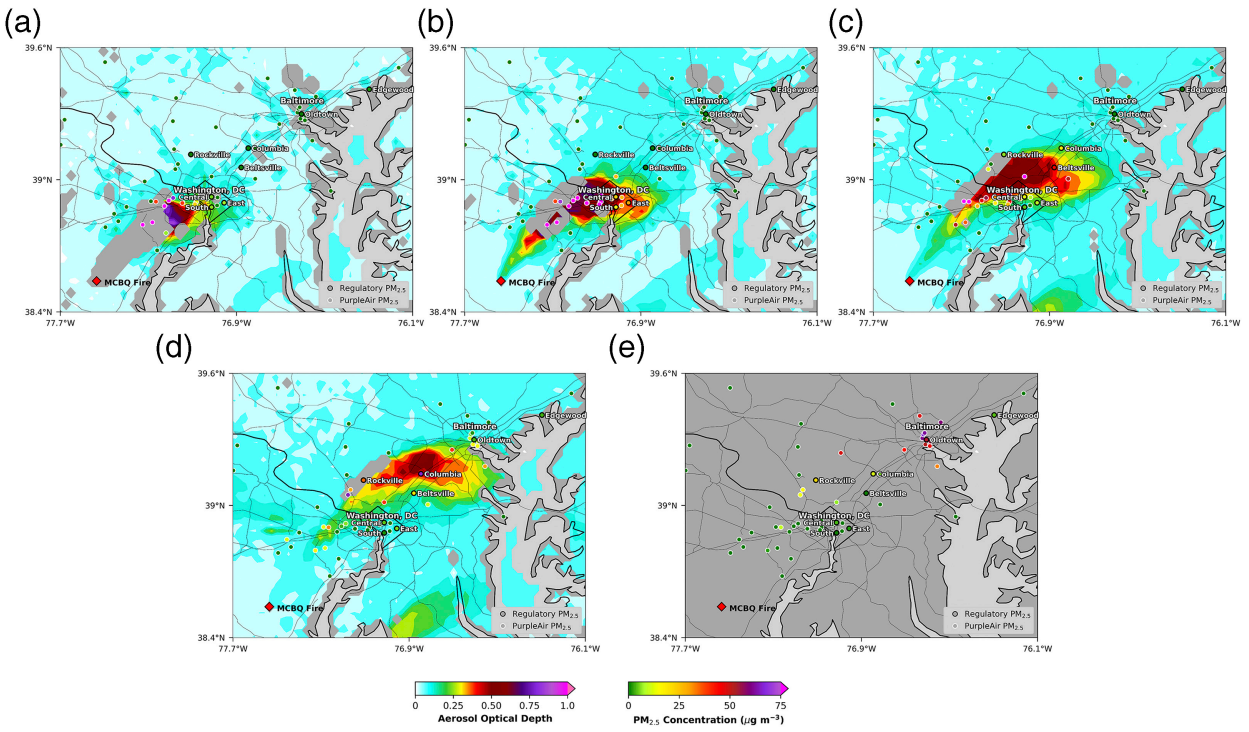

FIG. 7. 1-h composite *GOES-16* ABI AOD (top two qualities) overlaid with 1-h average $PM_{2.5}$ concentrations from regulatory monitors and PurpleAir sensors for (a) 1800, (b) 1900, (c) 2000, (d) 2100, and (e) 2200 UTC ($PM_{2.5}$ concentrations only; no AOD due to sunset) 8 Mar 2020. Also shown is the location of the prescribed fire on the lands of the MCBQ.

the MCBQ fire, and the south/southwesterly breeze and shallow PBL combined to funnel the smoke plume directly through the Baltimore–Washington corridor and concentrate it near the surface. With the backdrop of an otherwise clear, sunny, and clean day, the arrival of the plume in the DC metro area was noted by the public, with reports of reduced visibility, a strong smell, and coughing induced by the smoke (Samenow 2020).

There was no advance warning about the impacts of the smoke. Although MCBQ is located in Virginia, it is situated on federal land, so a state permit is not required to conduct prescribed burns. Consequently, the Virginia Department of Environmental Quality (DEQ) did not have prior knowledge of the controlled burn, so the DEQ's $PM_{2.5}$ air quality forecast did not include a warning to the public about the possibility of smoke in the area on 8 March (D. Salkovitz, Virginia Department of Environmental Quality, 2020, personal communication). In addition, no record of a public announcement of the controlled burn was found.

In the absence of advance notification regarding the fire, *GOES-16* ABI observations were the only way to determine the source of the smoke moving through the Baltimore–Washington corridor. The Baltimore–Washington NWS appears to have been the first to notify the public about the origin of the smoke via Twitter, after identifying the plume in ABI GeoColor imagery (Samenow 2020).

As demonstrated, ABI AOD CONUS sector observations with 5-min temporal resolution definitively captured the transport of the MCBQ plume along the Interstate 95 corridor in the afternoon of 8 March, moving from northern Virginia, through Washington, DC, across the Maryland suburbs, and to the southern edge of the Baltimore metro area from approximately 1800 to 2215 UTC. Ground-based measurements of $PM_{2.5}$ confirmed the deterioration of air quality conditions coincident with the progression of the plume.

The MCBQ smoke event illustrates the advantages of using multiple datasets to analyze the impacts of aerosols on ambient air quality. Although satellite AOD observations show the location of aerosols in two dimensions on the geographic scale, they cannot resolve the vertical distribution of aerosols in the atmosphere. In this case, the ceilometer aerosol backscatter measurements provide vertical information about the smoke that complements the geographic information from the ABI AOD data. The aerosol backscatter profiles confirm that the smoke extended from the surface to the top of the PBL during the times when ABI AOD indicate passage of the plume. Furthermore, ground-based $PM_{2.5}$ measurements verify that the smoke caused temporary deteriorations in surface air quality at the locations in the path of the plume. Only by combining data from all of these sources does a full picture emerge regarding the effects of the smoke plume transport.

A limitation of using ABI AOD to detect the smoke is lack of retrievals in the top 2 qualities AOD data. Missing AOD pixels are most egregious at 1800 UTC (Fig. 7a), when only the leading edge of the MCBQ plume is retrieved. At 1900 UTC (Fig. 7b), the issue is still substantial, with retrievals missing from the central portion of the plume over northern Virginia. The problem diminishes progressively at 2000 (Fig. 7c) and

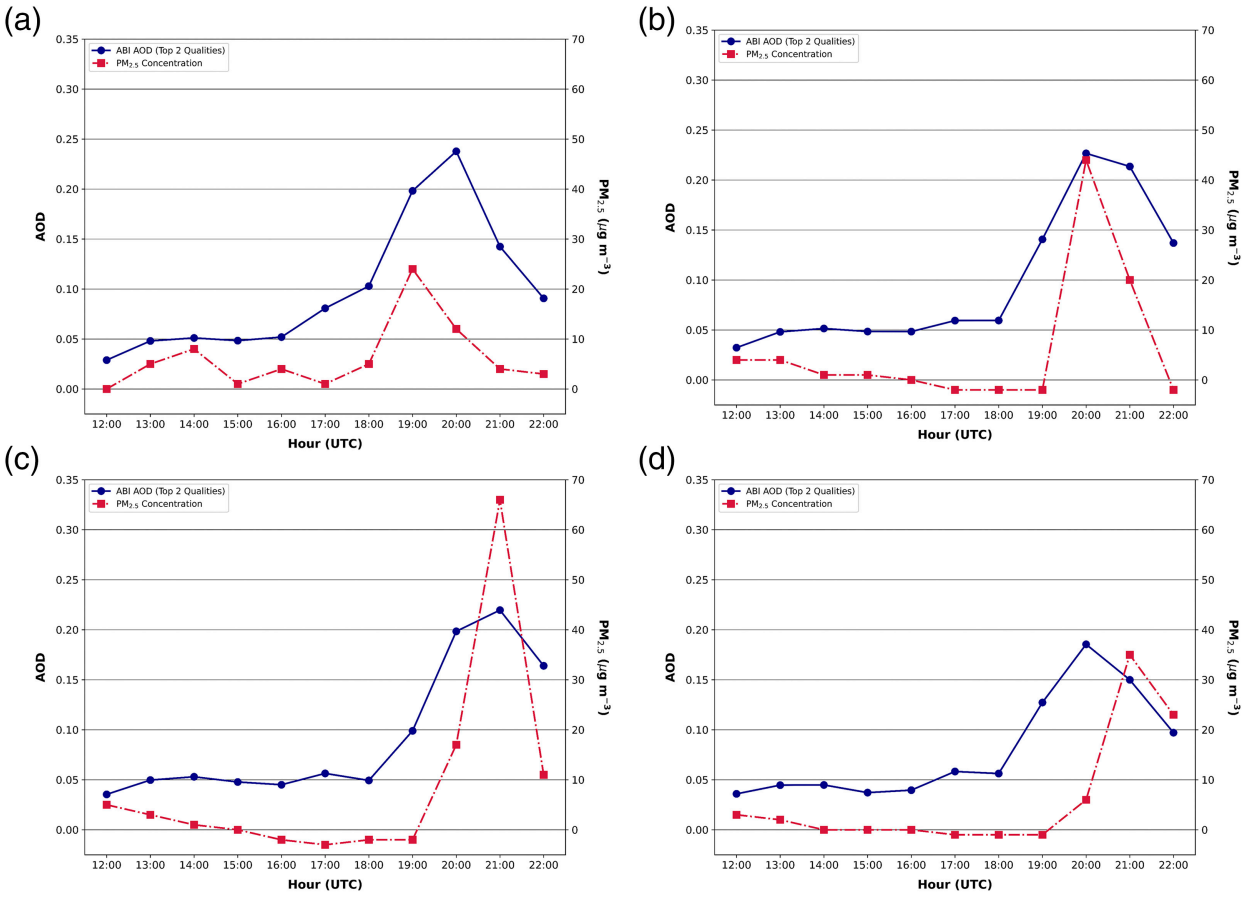

FIG. 8. Time series plots of 1-h average *GOES-16* ABI AOD and 1-h average $PM_{2.5}$ concentration from regulatory monitors at the (a) DC-Central, (b) Beltsville, (c) Columbia, and (d) Rockville sites on 8 Mar 2020.

2100 UTC (Fig. 7d), with missing pixels isolated to the western edge of the plume. Analysis of quality flags generated by the ABI AOD algorithm indicate that the missing pixels correspond to locations where the internal inhomogeneity test assigned AOD retrievals as low quality. The spatial inhomogeneity test checks for conditions that are unfavorable to accurate AOD retrievals, such as subpixel clouds or rugged terrain, by calculating the standard deviation (σ) at 0.47 μm (ABI band 1) over 2×2 pixels and 3×3 pixels. ABI AOD retrievals are designated low quality if $\sigma_{0.47\mu m} > 0.008$ with 1-km 0.47-μm reflectances over 2×2 pixels or $\sigma_{0.47\mu m} > 0.012$ with 2-km 0.47 μm reflectances over 3×3 pixels. In the case of the MCBQ plume, the spatial inhomogeneity flag is presumably triggered by highly reflective thicker smoke pixels adjacent to aerosol-free pixels, and these regions are being mistaken for subpixel clouds. Despite some portion of missing retrievals, top two qualities ABI AOD provides quantitative assessment of the smoke plume. All qualities ABI AOD (high, medium, and low) provides complete retrieval of the entire smoke plume at all time steps, with no missing pixels. Inclusion of low quality AOD comes at the expense of extensive erroneous high AOD retrievals in the analysis domain along coastal areas of the Chesapeake Bay and Potomac River, however.

Another shortcoming of using AOD to track aerosol movement is the need for visible light reflectances as input to the AOD algorithm. The last top 2 qualities ABI AOD observation over Baltimore on 8 March was at 2206 UTC, ahead of sunset at 2307 UTC (1937 EDT). As a result, the low sun angle in the hour prior to sunset and subsequent loss of sunlight prevented the complete monitoring of smoke transport through the Baltimore metro area from approximately 2200–2330 UTC, both by AERONET AOD at the Maryland Science Center site and by ABI AOD regionally. Although the evidence of surging $PM_{2.5}$ concentrations at the Oldtown monitor and surrounding PurpleAir sensors (Fig. 7e) indicates that the smoke plume did continue moving northeastward through Baltimore in the 2200–2300 UTC period, the progress of the plume could not be followed using AOD. There was no evidence in AOD or $PM_{2.5}$ measurements that the MCBQ plume was still present in the Baltimore–Washington corridor on 9 March.

A challenge in comparing satellite and point data is illustrated by the differences in the timing of the peaks of 1-h average ABI AOD and corresponding 1-h average $PM_{2.5}$ concentrations from the DC-Central (Fig. 8a) and Rockville (Fig. 8d) monitors. The 1-h lag between the maximum observed AOD and $PM_{2.5}$ at

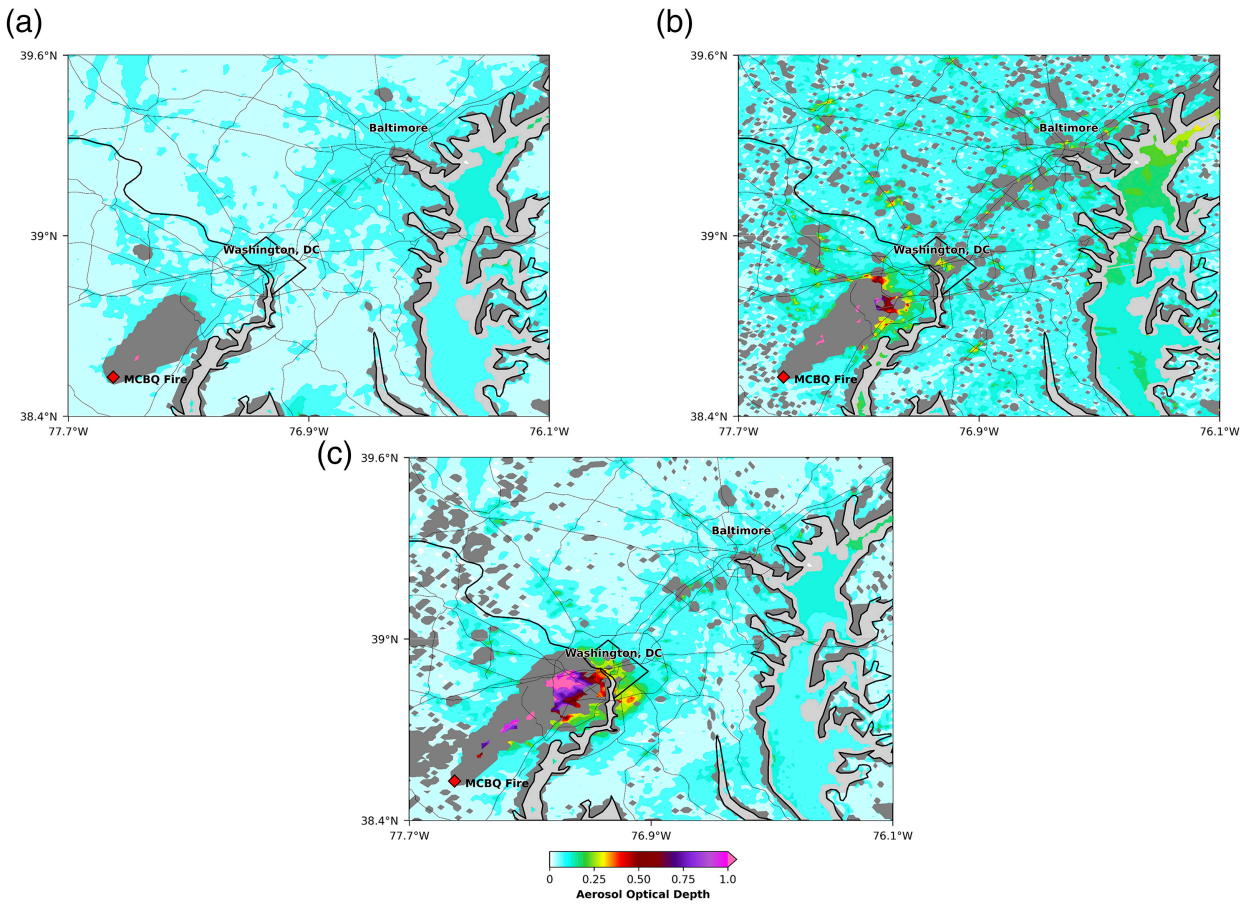

FIG. 9. VIIRS AOD (top two qualities) from (a) *NOAA-20* at 1704 UTC, (b) *SNPP* at 1752–1754 UTC, and (c) *NOAA-20* at 1844–1845 UTC 8 Mar 2020; also shown is the location of the prescribed fire on the lands of the MCBQ.

these sites is attributed to the area used to calculate the AOD spatial matchups in relation to the relatively small geographic extent of the smoke plume. A circle with radius of 27.5 km centered at the monitor site was chosen as the averaging area for ABI AOD in order to be consistent with standard practice for AOD AERONET matchups (Petrenko et al. 2012). At 1900 UTC, ABI AOD indicates the smoke plume encompassed DC (Fig. 7b), so the average AOD calculated within a circle with a 27.5-km radius centered on the DC-Central site is representative of the $PM_{2.5}$ concentration, which reached its maximum. At 2000 UTC, ABI AOD shows a sharp north–south gradient in the plume over DC, with thick smoke over northern DC, while central and southern DC are located on the periphery of the plume (Fig. 7c). As a result, the average AOD calculated within a circle with a 27.5-km radius centered on the DC-Central site at 2000 UTC includes high AOD values from northern DC, which pushed the spatially matched 1-h average ABI AOD to its maximum value. This AOD maximum was not fully representative of conditions at DC-Central, however, as the corresponding 1-h $PM_{2.5}$ concentration fell in response to the departure of the smoke to the north.

The opposite plume geography impacted the Rockville site. At 2000 UTC, Rockville was on the leading (northerly) edge of the smoke plume (Fig. 7c). Consequently, the average AOD calculated within a circle with a 27.5-km radius centered on the Rockville site at 2000 UTC includes high AOD values from the area south of the site, which pushed the spatially matched 1-h average ABI AOD to its maximum. Since the thickest part of the plume had not yet reached Rockville at 2000 UTC, the corresponding 1-h $PM_{2.5}$ concentration had not yet reached its maximum. At 2100 UTC, the smoke plume moved over the Rockville site (Fig. 7d), hence $PM_{2.5}$ reached its maximum. The thickest smoke had dispersed relative to the previous hour, however, so the spatially matched average AOD decreased slightly compared to 2000 UTC. These minor variations in peak AOD and $PM_{2.5}$ matchups at DC-Central and Rockville would not be expected for a larger smoke plume that covered a wider geographic area, or if a smaller AOD-averaging area were used.

AOD observations of the MCBQ smoke transport event were available from complementary instruments on polar-orbiting satellites, but they provided incomplete information. Neither NASA's Deep Blue (DB) nor Dark Target (DT) algorithms from the standard MOIDS Collection 6.1 product (10-km spatial resolution) retrieved the smoke plume; cloud masks and/or other filters excluded the pixels from both *Terra* (1555 UTC) and *Aqua* (1735 UTC). The DT MODIS 3-km

spatial resolution product did not detect the plume at all from *Aqua*, although a few pixels were retrieved from *Terra* along the leading edge of the plume, but not the center. Applied to VIIRS on *SNPP*, NASA's DB algorithm also was spotty, only retrieving two pixels near the center of the plume. Similarly, NOAA's VIIRS top two qualities AOD with 750-m spatial resolution at nadir (Fig. 9) showed uneven coverage of the plume; missing AOD is due to the internal inhomogeneity test assigning AOD retrievals as low quality and/or the external cloud mask misidentifying the smoke as cloud. There were three sets of VIIRS top two qualities AOD observations of the plume on 8 March. The first was on *NOAA-20* at 1704 UTC (Fig. 9a); only a few AOD pixels near the tail of the plume were detected. The next observations were from VIIRS on *SNPP* at 1752–1754 UTC (Fig. 9b). There were a few isolated AOD retrievals in the center of the plume, with sparse coverage of the leading edge of the plume. The second *NOAA-20* overpass at 1844–1845 UTC (Fig. 9c) provided the most complete AOD coverage, including much of the leading half of the plume, although most of the trailing half is missing.

Even if MODIS or VIIRS AOD had been able to resolve the smoke plume completely, these observations still only represent a snapshot of the event in the late morning (*Terra*) or early afternoon (*Aqua*, *SNPP*, and *NOAA-20*). AERONET AOD did capture the passage of the smoke at the GFSC station with high temporal resolution, as shown in Fig. 4, but AERONET is a point measurement, so it lacks the regional view provided by ABI AOD. Only the geostationary observations from *GOES-16* ABI were able to resolve the quickly evolving, regional smoke event on the time scale of 4–5 h in the afternoon of 8 March.

5. Conclusions

Analysis of the 8 March 2020 MCBQ event demonstrates the utility of ABI AOD for tracking the impacts of transported smoke aerosols on air quality. ABI AOD provides information for the public and decision-makers that is not available from any other source. Unlike AOD from instruments on polar-orbiting satellites, which are available only once or twice per day, the nearly continuous ABI AOD observations—every 5 min over the CONUS during daylight hours—enable monitoring of fast-evolving events on subdaily time scales, such as the MCBQ fire. Although AERONET AOD has the same high temporal resolution as ABI AOD, data from individual AERONET stations do not deliver the ABI's regional view, which allowed for surveillance of the MCBQ plume across the entire Baltimore–Washington corridor. While ABI GeoColor imagery provides visual confirmation of smoke on a regional scale, it is not a quantitative measure of aerosols like AOD. The quantitative aspect of AOD is critical for correlation with ground-based measurements, such as surface $PM_{2.5}$ concentrations.

Even with its current provisional maturity status, ABI AOD data provide valuable information to air quality and weather forecasters regarding the impacts of all types of atmospheric aerosols on air quality, not just smoke. There is a long history of using satellite AOD to estimate surface $PM_{2.5}$ concentrations (e.g., Hoff and Christopher 2009), which can be particularly useful for gauging the effects of large wildland fires or Saharan dust transport on air quality in locations outside of large metropolitan areas, where most regulatory pollutant monitors are clustered. A new method to estimate hourly $PM_{2.5}$ concentrations from AOD retrieved from the Advanced Himawari Imager (AHI) has been developed and utilized over Southeast Asia (Zhang and Kondragunta 2021). Application of this method to ABI AOD data is forthcoming, which will be an additional tool to assist operational air quality forecasters in assessing the mesoscale movement of polluted air masses, and it may be a valuable addition to EPA's NowCast calculation of current air quality conditions.

Acknowledgments. This work was supported by the NOAA JPSS program. The authors thank Ryan Auvil and Colleen Williams of MDE and Dr. Ram Tangirala of DOEE for providing $PM_{2.5}$ data and for helpful discussions. The scientific results and conclusions, as well as any views or opinions expressed herein, are those of the authors and do not necessarily reflect those of NOAA or the Department of Commerce.

Data availability statement. NWS sounding data are archived at the University of Wyoming's upper air sounding website (http://weather.uwyo.edu/upperair/sounding.html). Regulatory $PM_{2.5}$ data are available from EPA's Air Data website (https://www.epa.gov/outdoor-air-quality-data), and PurpleAir data can be downloaded from the PurpleAir website (https://www2.purpleair.com/). Raw and processed UCN ceilometer aerosol backscatter measurements at 10-min temporal resolution for 8 March 2020 are available at https://alg.umbc.edu/mcbq/. AERONET version 3 data can be downloaded using the AERONET Data Download Tool (https://aeronet.gsfc.nasa.gov/cgi-bin/webtool_aod_v3). *GOES-16* ABI AOD data files in netCDF format (available beginning July 25, 2018) can be ordered from NOAA's CLASS website (https://www.avl.class.noaa.gov/saa/products/welcome). Instructions for navigating CLASS to order and then download *GOES-16* ABI AOD data files are available in slide format at https://www.star.nesdis.noaa.gov/smcd/spb/aq/AerosolWatch/docs/CLASS-Tutorial_Feb2020.pptx or in video format at https://youtu.be/HkQcs7W1CD8.

REFERENCES

Achtemeier, G. L., 2009: On the formation and persistence of superfog in woodland smoke. *Meteor. Appl.*, **16**, 215–225, https://doi.org/10.1002/met.110.

Akagi, S. K., R. J. Yokelson, C. Wiedinmyer, M. J. Alvarado, J. S. Reid, T. Karl, J. D. Crounse, and P. O. Wennberg, 2011: Emission factors for open and domestic biomass burning for use in atmospheric models. *Atmos. Chem. Phys.*, **11**, 4039–4072, https://doi.org/10.5194/acp-11-4039-2011.

Caicedo, V., R. Delgado, R. Sakai, T. Knepp, D. Williams, K. Cavender, B. Lefer, J. Szykman, 2020: An automated common algorithm for planetary boundary layer retrievals using aerosol lidars in support of the U.S. EPA Photochemical Assessment Monitoring Sites program. *J. Atmos. Oceanic. Tech.*, **37**, 1847–1864, https://doi.org/10.1175/JTECH-D-20-0050.1.

Cazorla, A., and Coauthors, 2017: Near-real-time processing of a ceilometer network assisted with sun-photometer data: Monitoring a

dust outbreak over the Iberian Peninsula. *Atmos. Chem. Phys.*, **17**, 11 861–11 876, https://doi.org/10.5194/acp-17-11861-2017.

Ciren, P., and S. Kondragunta, 2014: Dust aerosol index (DAI) algorithm for MODIS. *J. Geophys. Res. Atmos.*, **119**, 4770–4792, https://doi.org/10.1002/2013JD020855.

Eck, T. F., B. N. Holben, J. S. Reid, O. Dubovik, A. Smirnov, N. T. O'Neill, I. Slutsker, and S. Kinne, 1999: Wavelength dependence of the optical depth of biomass burning, urban, and desert dust aerosols. *J. Geophys. Res.*, **104**, 31 333–31 349, https://doi.org/10.1029/1999JD900923.

Filonchyk, M., V. Hurynovich, and H. Yan, 2020: Trends in aerosol optical properties over eastern Europe based on MODIS-Aqua. *Geosci. Front.*, **11**, 2169–2181, https://doi.org/10.1016/j.gsf.2020.03.014.

Gupta, P., and Coauthors, 2018: Impact of California fires on local and regional air quality: The role of a low-cost sensor network and satellite observations. *Geohealth*, **2**, 172–181, https://doi.org/10.1029/2018GH000136.

Heese, B., H. Flentje, D. Althausen, A. Ansmann, and S. Frey, 2010: Ceilometer lidar comparison: Backscatter coefficient retrieval and signal-to-noise ratio determination. *Atmos. Meas. Tech.*, **3**, 1763–1770, https://doi.org/10.5194/amt-3-1763-2010.

Hoff, R. M., and S. A. Christopher, 2009: Remote sensing of particulate pollution from space: Have we reached the promised land? *J. Air Waste Manage. Assoc.*, **59**, 645–675, https://doi.org/10.3155/1047-3289.59.6.645.

Holben, B. N., and Coauthors, 1998: AERONET—A federated instrument network and data archive for aerosol characterization. *Remote Sens. Environ.*, **66**, 1–16, https://doi.org/10.1016/S0034-4257(98)00031-5.

Holder, A. L., A. K. Mebust, L. A. Maghran, M. R. McGown, K. E. Stewart, D. M. Vallano, R. A. Elleman, and K. R. Baker, 2020: Field evaluation of low-cost particulate matter sensors for measuring wildfire smoke. *Sensors*, **20**, 4796, https://doi.org/10.3390/s20174796.

Huang, J., and Coauthors, 2016: Validation and expected error estimation of Suomi-NPP VIIRS aerosol optical thickness and Ångström exponent with AERONET. *J. Geophys. Res. Atmos.*, **121**, 7139–7160, https://doi.org/10.1002/2016JD024834.

Jackson, J. M., H. Liu, I. Laszlo, S. Kondragunta, L. A. Remer, J. Huang, and H.-C. Huang, 2013: Suomi-NPP VIIRS aerosol algorithms and data products. *J. Geophys. Res. Atmos.*, **118**, 12 673–12 689, https://doi.org/10.1002/2013JD020449.

Johnston, F. H., and Coauthors, 2012: Estimated global mortality attributable to smoke from landscape fires. *Environ. Health Perspect.*, **120**, 695–701, https://doi.org/10.1289/ehp.1104422.

Kondragunta, S., I. Laszlo, H. Zhang, P. Ciren, and A. Huff, 2020: Air quality applications of ABI aerosol products from the GOES-R series. *The GOES-R Series: A New Generation of Geostationary Environmental Satellites*, S. J. Goodman et al., Eds., Elsevier, 203–217.

Koplitz, S. N., C. G. Nolte, G. A. Pouliot, J. M. Vukovich, and J. Beidler, 2018: Influence of uncertainties in burned area estimates on modeled wildland fire PM2.5 and ozone pollution in the contiguous US. *Atmos. Environ.*, **191**, 328–339, https://doi.org/10.1016/j.atmosenv.2018.08.020.

Kumar, K. R., Y. Yin, V. Sivakumar, N. Kang, X. Xu, Y. Diao, A. J. Adesina, and R. R. Reddy, 2015: Aerosol climatology and discrimination of aerosol types retrieved from MODIS, MISR and OMI over Durban (29.88°S, 31.02°E), South Africa. *Atmos. Environ.*, **117**, 9–18, https://doi.org/10.1016/j.atmosenv.2015.06.058.

Larkin, N. K., S. M. Raffuse, S.-M. Huang, N. Pavlovic, P. Lahm, and V. Rao, 2020: The Comprehensive Fire Information Reconciled Emissions (CFIRE) inventory: Wildland fire emissions developed for the 2011 and 2014 U.S. National Emissions Inventory. *J. Air Waste Manage. Assoc.*, **70**, 1165–1185, https://doi.org/10.1080/10962247.2020.1802365.

Lassman, W. B., R. W. Ford, G. Gan, S. Pfister, E. V. Magzamen, J. R. Fischer, and J. R. Pierce, 2017: Spatial and temporal estimates of population exposure to wildfire smoke during the Washington State 2012 wildfire season using blended model, satellite, and in situ data. *Geohealth*, **1**, 106–121, https://doi.org/10.1002/2017GH000049.

Laszlo, I., and H. Liu, 2017: EPS aerosol optical depth (AOD): Version 3.0.4. NOAA NESDIS Center for Satellite Applications and Research Algorithm Theoretical Basis Doc., 77 pp., https://www.star.nesdis.noaa.gov/smcd/spb/aq/AerosolWatch/docs/JPSS_VIIRS_EPS_AOD_ATBD_V3.0.4_20170106.pdf.

——, P. Ciren, H. Liu, S. Kondragunta, J. D. Tarpley, and M. D. Goldberg, 2008: Remote sensing of aerosol and radiation from geostationary satellites. *Adv. Space Res.*, **41**, 1882–1893, https://doi.org/10.1016/j.asr.2007.06.047.

Levy, R. C., L. A. Remer, S. Mattoo, E. F. Vermote, and Y. J. Kaufman, 2007: Second-generation operational algorithm: Retrieval of aerosol properties over land from inversion of Moderate Resolution Imaging Spectroradiometer spectral reflectance. *J. Geophys. Res.*, **112**, D13211, https://doi.org/10.1029/2006JD007811.

——, ——, R. G. Kleidman, S. Mattoo, C. Ichoku, R. A. Kahn, and T. F. Eck, 2010: Global evaluation of the collection 5 MODIS dark-target aerosol products over land. *Atmos. Chem. Phys.*, **10**, 10 399–10 420, https://doi.org/10.5194/acp-10-10399-2010.

——, S. Mattoo, L. A. Munchak, L. A. Remer, A. M. Sayer, and N. C. Hsu, 2013: The Collection 6 MODIS aerosol products over land and ocean. *Atmos. Meas. Tech.*, **6**, 2989–3034, https://doi.org/10.5194/amt-6-2989-2013.

Liu, H., L. A. Remer, J. Huang, H.-C. Huang, S. Kondragunta, I. Laszlo, M. Oo, and J. M. Jackson, 2014: Preliminary evaluation of S-NPP VIIRS aerosol optical thickness. *J. Geophys. Res.*, **119**, 3942–3962, https://doi.org/10.1002/2013JD020360.

Petrenko, M., C. Ichoku, and G. Leptoukh, 2012: Multi-sensor Aerosol Products Sampling System (MAPSS). *Atmos. Meas. Tech.*, **5**, 913–926, https://doi.org/10.5194/amt-5-913-2012.

Rappold, A. G., and Coauthors, 2011: Peat bog wildfire smoke exposure in rural North Carolina is associated with cardiopulmonary emergency department visits assessed through syndromic surveillance. *Environ. Health Perspect.*, **119**, 1415–1420, https://doi.org/10.1289/ehp.1003206.

Samenow, J., 2020: Controlled burn near Quantico causes smoke conditions across Washington region. *Washington Post*, 8 March 2020, https://www.washingtonpost.com/weather/2020/03/08/controlled-burn-near-quantico-causes-smoky-conditions-across-washington-region/.

Sapkota, A., and Coauthors, 2005: Impact of the 2002 Canadian forest fires on particulate matter air quality in Baltimore City. *Environ. Sci. Technol.*, **39**, 24–32, https://doi.org/10.1021/es035311z.

Schmit, T. J., P. Griffith, M. M. Gunshor, J. M. Daniels, S. J. Goodman, and W. J. Lebair, 2017: A closer look at the ABI on the GOES-R series. *Bull. Amer. Meteor. Soc.*, **98**, 681–698, https://doi.org/10.1175/BAMS-D-15-00230.1.

Stanaway, J. D., and Coauthors, 2018: Global, regional, and national comparative risk assessment of 84 behavioural, environmental and occupational, and metabolic risks or clusters of risks for 195 countries and territories, 1990–2017: A systematic analysis for the Global Burden of Disease study 2017.

Lancet, **392**, 1923–1994, https://doi.org/10.1016/S0140-6736(18)32225-6.

U.S. Government, 2017: Network design criteria for ambient air quality monitoring. U.S. Code of Federal Regulations 40, Part 58, Appendix D, 295–310, https://www.govinfo.gov/app/details/CFR-2019-title40-vol6/CFR-2019-title40-vol6-part58-appD.

Weber, S. A., T. Z. Insaf, E. S. Hall, T. O. Talbot, and A. K. Huff, 2016: Assessing the impact of fine particulate matter ($PM_{2.5}$) on respiratory-cardiovascular chronic diseases in the New York City metropolitan area using hierarchical Bayesian model estimates. *Environ. Res.*, **151**, 399–409, https://doi.org/10.1016/j.envres.2016.07.012.

Wiedinmyer, C., B. Quayle, C. Geron, A. Belote, D. McKenzie, X. Y. Zhang, S. O'Neill, and K. K. Wynne, 2006: Estimating emissions from fires in North America for air quality modeling. *Atmos. Environ.*, **40**, 3419–3432, https://doi.org/10.1016/j.atmosenv.2006.02.010.

Zhang, H., and S. Kondragunta, 2021: Daily and hourly surface PM2.5 estimation from satellite AOD. *Earth Space Sci.*, **8**, e2020EA001599, https://doi.org/10.1029/2020EA001599.

——, ——, I. Laszlo, and M. Zhou, 2020: Improving GOES Advanced Baseline Imager (ABI) aerosol optical depth (AOD) retrievals using an empirical bias correction algorithm. *Atmos. Meas. Tech.*, **13**, 5955–5975, https://doi.org/10.5194/amt-13-5955-2020.